Inorganic Chemistry

pubs.acs.org/IC Article

Linear versus Bent Uranium(II) Metallocenes—A Local Vibrational Mode Study

Bárbara M. T. C. Peluzo, Małgorzata Z. Makoś, Renaldo T. Moura, Jr., Marek Freindorf, and Elfi Kraka*

Cite This: *Inorg. Chem.* 2023, 62, 12510−12524 Read Online

ACCESS | Metrics & More | Article Recommendations | Supporting Information

ABSTRACT: Uranium metallocenes have recently attracted attention driven by their use as catalysts in organometallic synthesis. In addition to bent U(IV) and U(III), an U(II) metallocene $[(\eta^5\text{-}C_5^i\ Pr_5)_2U]$ was synthesized with an unusual linear Cp−U−Cp angle. In this work, we investigated 22 U(II) metallocenes, (i) assessing the intrinsic strength of the U-ring interactions in these complexes with a novel bond strength measure based on our local vibrational mode analysis and (ii) systematically exploring what makes these U(II) metallocenes bent. We included relativistic effects through the NESCau Hamiltonian and complemented the local mode analysis with natural bonding orbital (NBO) and quantum theory of atoms in molecules (QTAIM) data. Our study led to the following results: (i) reduction of bulky U-ring ligand substituents does not lead to bent complexes for alkyl substituents (^{i}Pr and ^{i}Bu) in contrast to $SiMe_3$ ring substituents, which are all bent. (ii) The most bent complexes are $[(\eta^5\text{-}C_5H_4SiMe_3)_2U]$ (130°) and $[\eta^5\text{-}P_5H_5)_2U]$ (143°). (iii) Linear complexes showed one hybridized NBO with s/d character, while bent structures were characterized by s/d/f mixing. (iv) We did not observe a correlation between the strength of the U-ring interaction and the amount of the ring-U-ring bend; the strongest interaction was found for $[\eta^5\text{-}Cp)_2U]$ and the weakest for $[\eta^5\text{-}P_5H_5)_2U]$. In conclusion, our results provide a foundation for the design of U(II) metallocenes with specific physicochemical properties and increased reactivity.

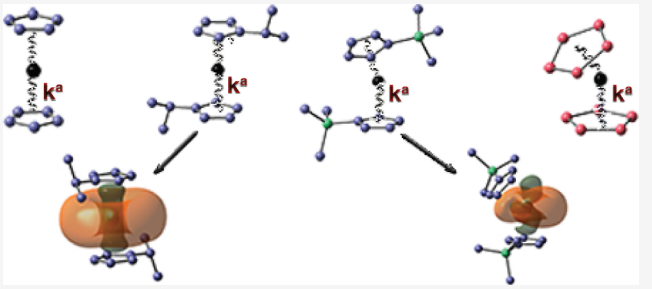

INTRODUCTION

Uranocene, $(\eta^8\text{-}C_8H_8)_2U$ (**1**, Figure 1), is the most prominent and studied member of the actinide sandwich complex family. **1** is often regarded as the archetype actinocene since its first synthesis in the late 1960s.[1] One of the most intriguing structural aspects of this U(IV) π−bonded sandwich complex is its high D_{8h} symmetry with eclipsed cyclooctatetraenide (COT) ligands and a COT−U−COT angle of 180°.

Subsequently, U(IV) derivatives of **1** were synthesized, e.g., substituting one COT ligand with two Si^iPr_3 (tri-isopropylsilyl) groups and replacing the other COT with cyclopentadienyl (Cp) substituted with one ^{t}Bu (tertiary butyl) group,[2] reducing the oxidation state of uranium to U(III) (**2**, Figure 1). In addition to Cp ligands, cyclobutadienyl (Cb) ligands were reported resulting in bent U(III) metallocenes as well (**3**, Figure 1).[3] Interesting to note is that such bulky substituents were needed to isolate this compound. A 1,3,5-trimethyl-1,3,5-triazacyclohexane (Me_3tach) ligand was recently applied for the first time in the synthesis of U(III) complexes with metallocenes-like structures.[4]

In 2013, the first stable U(II) complex was isolated in the form of $[Cp_3'\ U]^-$, with Cp′ = $C_5H_3(SiMe_3)$.[5] In addition to U(IV) and U(III) metallocenes,[6] a stable U(II) $[\eta^5\text{-}C_5^i\ Pr_5)_2U]$ sandwich complex was isolated with a linear Cp-U-Cp angle (**4**, Figure 1), which was explained via the hybridization between $6d_{z^2}$ and 7s orbitals,[7] in line with other reports that the uranium atom preferentially adopts a valence configuration of $5f^36d^1$ in U(II) sandwich complexes[8] but that a $5f^4$ configuration is also possible when U-ligand bonding is stabilized via δ back-bonding.[9] While this work has been in progress, the first U(I) sandwich complex (**5**, Figure 1), obtained through the reduction of **1**, has been added to the repertoire.[10] It is important to note that such a compound assumes a bent arrangement.

As an alternative to Cp ring ligands, metal sandwich complexes with phosphorus-containing ring ligands have been reported in the mid-90s such as 1,3-diphospholides (C_3P_2) η^5 sandwich complexes with molybdenum,[11] as well as phospholides (C_4P) yttrium, samarium, and lutetium η^5 coordination compounds.[12,13] Likewise, U(IV) and U(III) metallocenes with phospholides (C_4P) rings substituted with methyl groups were experimentally observed.[14−16] Recently, an inorganic version of ferrocene, $[(\eta^4\text{-}P_4)_2Fe]^{2-}$, was experimentally observed.[17] However, to our best knowledge no

Received: May 29, 2023
Published: July 21, 2023

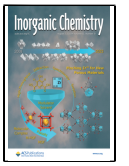

https://doi.org/10.1021/acs.inorgchem.3c01761
Inorg. Chem. 2023, 62, 12510−12524

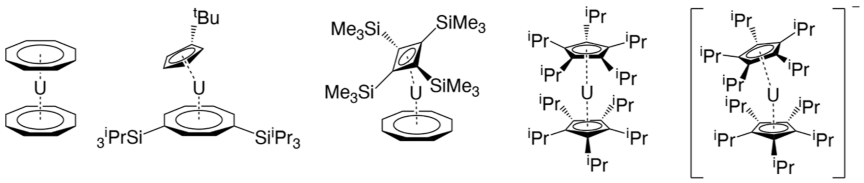

Figure 1. Examples of synthesized linear and bent uranium sandwich complexes.

corresponding $[(\eta^4\text{-}P_4)_2]$ or $[(\eta^5\text{-}P_5)_2]$ uranocene has been synthesized so far.

It has been observed that bent uranocenes show reductive properties,[18] selectivity,[4,19] and an overall increased reactivity compared to their linear counterparts, making them favorable candidates for catalysis.[19−21] For example, bent U(III) containing COT and Cp rings exhibited higher reactivity/selectivity toward CO and CO_2 than their linear counterparts with highly substituted COT and Cp rings.[2,3] It was speculated that changing the geometry of a sandwich complex from linear to bent obviously changes the physicochemical properties of the complex, the steric interactions between the ring ligands, and most important the electronic nature of U-ring bonding.[22] In this connection, the difference between electron-withdrawing silyl versus electron-donating alkyl substituents was pointed out.[23] It has been further suggested that complex bending is caused by increased covalent character of U-ring bonding, however without providing a systematic and quantitative assessment of the nature and strength of the U-ring interaction.[2,20,24] In particular, a systematic assessment of (i) the nature and strength of the metal-ring interaction in U(II) metallocenes and (ii) what induces bent or linear structures has not been reported so far to our best knowledge.

In order to systematically address these two questions, we investigated in this work 22 U(II) sandwich complexes (starting from **4**), divided into four groups shown in Figure 2. Group I complexes **G1.0**−**G1.5** explored the question of whether systematic removal of the bulky electron-donating ^{i}Pr ring substituents would lead to bent complexes. The same question was addressed for Group II members **G2.1**−**G2.4** with even bulkier ^{t}Bu ring substituents. In Group III complexes **G3.1**−**G3.4**, we investigated the effect of electron-withdrawing $SiMe_3$ ring substituents, which obviously led to bent structures in the case of **2** and **3**. Inspired by the synthesis of the first inorganic ferrocene analogue ($[(\eta^4\text{-}P_4)_2Fe]^{2-}$),[17] we investigated in Group IV potential U(II) metallocenes **G4.1**−**G4.8**, with phosphorous Cp analogues, the so-called phosphacyclopentadienyls with $P_n{-}C_{5-n}$ (n = 1···5) being substituted with Et (ethyl), ^{t}Bu, and/or $SiMe_3$. Phosphacyclo-pentadienyl ligands are known for their wide synthetic versatility, in particular in coordination chemistry.[25−27]

The article is organized as follows. In the next section, computational details are provided, including a brief description of (i) the relativistic Hamiltonian NESCau applied in this work, (ii) the local vibrational mode analysis (LMA) and the associated bond strength measure utilized to assess the strength of U-ring interaction, and (iii) how the covalent character of this interaction was determined. Then our results are discussed, focusing first on structural and steric aspects, followed by electronic effects and their interplay with steric effects, including the assessment of the strength of the U-ring interaction via local mode force constants and their covalent character via the energy density $H(\mathbf{r})$ and an inspection of the

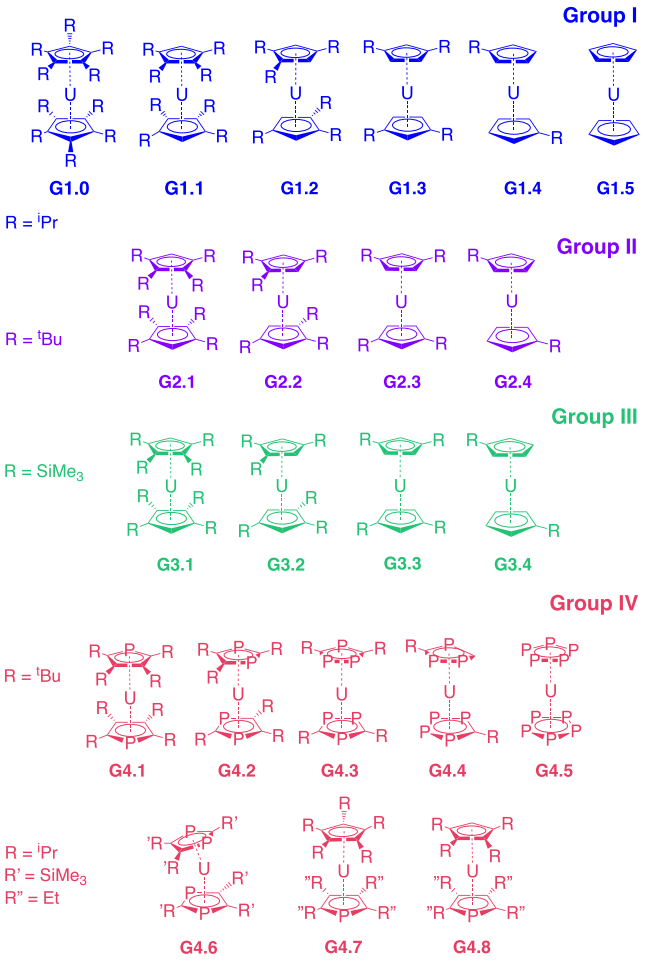

Figure 2. Uranium divalent metallocenes studied in this work.

Laplacian of the electron density $\rho(\mathbf{r})$ in the bonding region. The quantum theory of atoms in molecules (QTAIM) discussion is complemented by a natural bonding orbital (NBO) analysis, focusing on the correlation between 5f orbital occupation and complex structure. The article closes with conclusions and some general remarks.

COMPUTATIONAL DETAILS

NESCau Relativistic Hamiltonian. The theoretical description of uranium requires a careful treatment of relativistic effects that make sizable or even dominant contributions to molecular properties of uranium compounds, in particular uranium−ligand bonding. Effective core potentials, which are widely used to describe relativistic effects in DFT calculations,[28] consider valence electrons in the non-relativistic picture and were previously associated with non-negligible errors in calculations involving large variations of oxidation states.[29]

https://doi.org/10.1021/acs.inorgchem.3c01761
Inorg. Chem. 2023, 62, 12510−12524

Our Dirac-exact NESC (normalized elimination of the small component) method[30,31] is a Dirac-exact two-component (2c) relativistic approach[32] belonging to the X2C family,[31,33] i.e., a method that is capable of reproducing the one-electron results from the original four-component (4c) Dirac equation. The Dirac-exact NESC methodology allows for accurate calculations of first- and second-order response properties, including vibrational frequencies and spin−orbit coupling via the screened nuclear spin−orbit approximation,[32,34−38] for a variety of DFT and correlation-corrected wave function methods, thus guaranteeing a broad application range.[30,39] To the best of our knowledge, current X2C releases, e.g., the Cheng and Gauss approach, provide analytic first-[40] and second-order[41] derivatives, nonetheless at the spin-free level. We recently expanded NESC to an atomic unitary transformation (NESCau), which allows for efficient 2c calculations of relativistic effects in large systems,[33] qualifying NESCau as the optimal choice for this project, given the large size of the systems under study and the unusual oxidation state of uranium. It should be mentioned that the nomenclature X2Cau, employed by Zou et al.,[32] is a synonym for NESCau.

Detailed descriptions of both NESC and NESCau have been previously reported.[30−32] Henceforth, this section aims at providing an overview of NESCau's main aspects. The starting point is a modified 4c-Dirac equation,[42] with the usual split into large Ψ and small Φ components

$$\begin{aligned}(V-E)\Psi + T\Phi &= 0\\ T\Psi + \left[\frac{\alpha^2}{4}(\boldsymbol{\sigma}\cdot\boldsymbol{p})(V-E)(\boldsymbol{\sigma}\cdot\boldsymbol{p}) - T\right]\Phi &= 0\end{aligned} \tag{1}$$

where V and T account for potential and kinetic energy, $\boldsymbol{\sigma}$ contains Pauli spin matrices, $\boldsymbol{p}$ is the linear momentum vector, and E is the energy eigenvalues. The restricted kinetic balance allows for the obtainment of Φ after Ψ. Expansion of both Ψ and Φ on a basis leads to eq 1 on its matrix form

$$\begin{pmatrix}\mathbf{V} & \mathbf{T}\\ \mathbf{T} & \frac{\alpha^2}{4}\mathbf{W}-\mathbf{T}\end{pmatrix}\begin{pmatrix}\mathbf{A}\\ \mathbf{B}\end{pmatrix} = \begin{pmatrix}\mathbf{S} & 0\\ 0 & \frac{\alpha^2}{2}\mathbf{T}\end{pmatrix}\begin{pmatrix}\mathbf{A}\\ \mathbf{B}\end{pmatrix}E \tag{2}$$

where $\mathbf{W} = (\boldsymbol{\sigma}\cdot\boldsymbol{p})V(\boldsymbol{\sigma}\cdot\boldsymbol{p})$, and $\mathbf{S}$ is the overlap matrix. One can write $\mathbf{B}$ in terms of $\mathbf{A}$

$$\mathbf{B} = \mathbf{U}\mathbf{A} \tag{3}$$

where $\mathbf{U}$ is a nonunitary transformation matrix given by

$$\mathbf{U} = \mathbf{T}^{-1}[\mathbf{S}E - \mathbf{V}] \tag{4}$$

Following algebraic manipulations lead to expressions for modified kinetic

$$\tilde{\mathbf{T}} = \mathbf{T}\mathbf{U} + \mathbf{U}^{\dagger}\mathbf{T} - \mathbf{U}^{\dagger}\mathbf{T}\mathbf{U} \tag{5}$$

and potential energies

$$\tilde{\mathbf{V}} = \mathbf{V} + \frac{\alpha^2}{4}\mathbf{U}^{\dagger}\mathbf{W}\mathbf{U} \tag{6}$$

and a modified overlap matrix

$$\tilde{\mathbf{S}} = \mathbf{S} + \frac{\alpha^2}{2}\mathbf{U}^{\dagger}\mathbf{T}\mathbf{U} \tag{7}$$

$\tilde{\mathbf{T}}$, $\tilde{\mathbf{V}}$, and $\tilde{\mathbf{S}}$ comprise the NESC Hamiltonian $\tilde{\mathbf{L}}$ and its eigenvalue equation

$$(\tilde{\mathbf{T}} + \tilde{\mathbf{V}})\mathbf{A} = \tilde{\mathbf{L}}\mathbf{A} = \tilde{\mathbf{S}}\mathbf{A}E \tag{8}$$

where $\tilde{\mathbf{L}}$ is normalized through the relativistic metric $\tilde{\mathbf{S}}$. The extension to the many electrons systems requires a renormalization

$$\mathbf{H}^{\mathrm{NESC}} = \mathbf{G}^{\dagger}\tilde{\mathbf{L}}\mathbf{G} \tag{9}$$

where $\mathbf{H}^{\mathrm{NESC}}$ replaces the Fock matrix on the SCF cycle. $\tilde{\mathbf{G}}$ is a nonrelativistic metric given by

$$\mathbf{G} = \mathbf{S}^{-1/2}\mathbf{K}\mathbf{S}^{1/2} \tag{10}$$

and

$$\mathbf{K} = (\mathbf{S}^{-1/2}\tilde{\mathbf{S}}\mathbf{S}^{-1/2})^{-1/2} \tag{11}$$

Matrix $\mathbf{U}$ is the core foundation of NESC, and it is calculated iteratively in the original NESC formulation. Notwithstanding, its computation is a critical drawback as it gets demanding as system size increases, preventing the use of NESC on larger systems. Based on the fact that most of the relativistic effects take place locally,[43] we can further approximate $\mathbf{U}$ and $\mathbf{G}$ as direct sums of atomic matrices $\mathbf{U}_A$

$$\mathbf{U} \approx \sum^{\oplus} \mathbf{U}_A \tag{12}$$

and $\mathbf{G}_A$

$$\mathbf{G} \approx \sum^{\oplus} \mathbf{G}_A \tag{13}$$

Equations 12 and 13 define the NESCau method, which allows for the inclusion of relativistic effects in larger systems, achieving a good compromise between accuracy and efficiency. Highly accurate results obtained with NESCau were reported on the study of actinide sandwich complexes[33] and uranium molecules featuring multiple bonds.[44]

Local Vibrational Mode Analysis. LMA originally developed by Konkoli and Cremer[45] has become over the past years a versatile tool for extracting important chemical information from vibrational spectroscopy data, often being hidden because of the very nature of normal vibrational modes, namely being delocalized in polyatomic molecules.[46,47] LMA has led to both a new quantitative measure of bond strength based on local mode force constants[48] and a new way to analyze vibrational spectra, the so-called composition of normal mode (CNM) analysis.[49] The underlaying theory as well as a comprehensive overview of LMA applications have been published in two recent review articles;[50,51] therefore, in the following, only some essentials of LMA are summarized.

The starting point is the Wilson equation of spectroscopy[46] for a system containing N vibrating atoms

$$\mathbf{F}^{x}\tilde{\mathbf{L}} = \mathbf{M}\tilde{\mathbf{L}}\mathbf{\Lambda} \tag{14}$$

where $\mathbf{F}$ is the force constant matrix (i.e., Hessian) in Cartesian coordinates x, $\tilde{\mathbf{L}}$ is the matrix that collects the normal vibrational vectors (here denoted by $\tilde{\mathbf{I}}_{\mu}$) in Cartesian coordinates column-wise and $\mathbf{M} = \mathrm{diag}(m_1, m_1, m_1, \ldots, m_i, m_i, m_i, \ldots, m_N, m_N, m_N)$, i.e., a diagonal mass matrix in which each atomic mass m_i appears three times. $\mathbf{\Lambda}$, on its turn, is a diagonal matrix containing λ_{μ} eigenvalues, which are related to the harmonic vibrational frequencies ω_{μ} through $\lambda_{\mu} = 4\pi^2c^2\omega_{\mu}^2$ (c is the speed of light). The tilde symbols above $\mathbf{L}$ and $\mathbf{I}$ account for mass-weighting, whereas the superscript x denotes the use of Cartesian coordinates. Renormalization of the normal mode vectors $\tilde{\mathbf{I}}$ and subsequent diagonalization of eq 14 leads to

https://doi.org/10.1021/acs.inorgchem.3c01761
Inorg. Chem. 2023, 62, 12510−12524

transformation from Cartesian to normal coordinates **Q** and the diagonal force constant matrix **K**.[46]

It is often more convenient to express the molecular geometry in terms of N_{vib} internal coordinates q (with $N_{vib} = 3N - 5$ for linear and $3N - 6$ for non-linear molecules) rather than $3N$ Cartesian coordinates x. Doing so, the Wilson equation adopts the following form[46]

$$\mathbf{F}^q\mathbf{D} = \mathbf{G}^{-1}\mathbf{D}\mathbf{\Lambda} \tag{15}$$

where **D** collects the normal mode vectors $\mathbf{d}_n$ (n = 1, ..., N_{vib}) column-wise. The Wilson **G** matrix

$$\mathbf{G} = \mathbf{B}\mathbf{M}^{-1}\mathbf{B}^{\dagger} \tag{16}$$

represents the kinetic energy in terms of internal coordinates. The elements of the **B** matrix in eq 16 are defined by the partial derivatives of internal coordinates with regard to Cartesian coordinates. It is important to note that the **B** matrix plays a central role in the Wilson equation of spectroscopy, namely connecting different sets of coordinates (internal, symmetry, curvilinear, etc.) with the Cartesian coordinates.[46] Therefore, whenever a new set of coordinates is introduced, the first step is to derive the appropriate **B** matrix. This is an important point for deriving a new bond strength measure for metal-ring interactions, as discussed below.

Vector $\mathbf{d}_n$ and diagonal force constant matrix **K** (the standard output of a normal mode analysis performed in most modern quantum chemistry packages) are the only ingredients needed to derive local mode vector $\mathbf{a}_n$

$$\mathbf{a}_n = \frac{\mathbf{K}^{-1}\mathbf{d}_n^{\dagger}}{\mathbf{d}_n\mathbf{K}^{-1}\mathbf{d}_n^{\dagger}} \tag{17}$$

and the corresponding local mode force constant k_n^a is defined as

$$k_n^a = \mathbf{a}_n^{\dagger}\mathbf{K}\mathbf{a}_n = \frac{1}{\mathbf{d}_n\mathbf{K}^{-1}\mathbf{d}_n^{\dagger}} \tag{18}$$

In a recent work,[52] we derived a unique local mode stretching force constant for the quantitative description of metal−π interactions, a necessary prerequisite for a detailed understanding and assessment of how these interactions influence molecular properties and reactivity, an important tool, which so far is still missing. One could think of calculating the local modes for all M-ring atom interactions and averaging over the corresponding local mode force constants. However, such an averaged local force constant leads to redundancies as shown in ref 52. Therefore, the use of one interaction parameter is not only physically meaningful, but it also characterizes the collective effects of the whole π-system. In this study, we used the local stretching force constant k^a(U−X′) between uranium and the ring center X′ (see Figure 3a) and the local mode force constant k^a(X′−U−X′) associated with the angle between the ring centers and uranium (see Figure 3b).

For the comparison of a large number of k^a(U−X′) values, it is convenient to resort to relative bond strength orders (BSO n) which can be derived from local mode force constants via a generalized Badger rule[53,54]

$$\text{BSO } n = u[k^a(\text{U} - \text{X}')]^v \tag{19}$$

u and v are defined via two reference molecules with known BSO n and k^a(U−X′) values and the request that a zero value of k^a(U−X′) implies a zero BSO n value. For metal−ligand

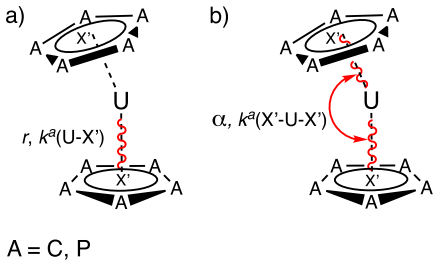

Figure 3. (a) Definition of the local mode parameter r and local mode force constant k^a(U−X′) describing the U−X′ ring interaction. (b) Definition of the local mode parameter α and related local mode force constant k^a(X′−U−X′) describing (X′−U−X′) angle.

interactions, it is appropriate to use the Mayer bond order[55−57] to obtain BSO n values for the reference molecules: the Mayer bond order for the single bond is set to a BSO n value of 1 and the double bond value is scaled accordingly. In this work, we used H_3C−UH and H_2C=UH_2 as reference molecules for uranium-carbon single and double bonds, respectively. The corresponding k^a values, calculated with the PBE0/NESCau level of the theory with cc-pVDZ and SARC-DKH2(U) basis sets, are 1.409 mdyn/Å (single bond) and 3.355 mdyn/Å (double bond) with corresponding single and double bond lengths of 2.3653 and 2.0230 Å, respectively. These values are in good agreement with the previously published results.[58,59] The corresponding scaled Mayer bond orders of 1 and 1.983 for single and double bonds (unscaled values: 0.981 and 1.945) led to 0.7629 and 0.7891 for u and v, respectively. Equation 19 was applied for both uranium−Cp and uranium−phospholide interactions. In essence, BSO n translates the local force constant into a chemically more cogent and understandable bond strength measure.[54]

Topological Analysis of the Electronic Density. The quantum theory of atoms in molecules (QTAIM)[60−63] was utilized to evaluate the covalent character of uranium−ring interactions. According to the Cremer−Kraka criterion,[64−66] the energy density $H(\mathbf{r}_b)$

$$H(\mathbf{r}_b) = G(\mathbf{r}_b) + V(\mathbf{r}_b) \tag{20}$$

evaluated at the bond critical point, $\mathbf{r}_b$, is a measure of the covalent character of a chemical bond or weak chemical interaction.[64−66] $\mathbf{r}_b$ is defined as the (3, −1) saddle point of electronic density $\rho(\mathbf{r})$ along the bond path between the two atoms under consideration. Its occurrence is the necessary condition of the Cremer−Kraka criterion ($G(\mathbf{r}_b)$ and $V(\mathbf{r}_b)$ in eq 20, account for the kinetic and potential energy densities, respectively). The sufficient condition for predominant covalent character of the chemical bond or weak chemical interaction is a negative value of $H(\mathbf{r}_b)$, i.e., $V(\mathbf{r}_b)$ predominates over the positive $G(\mathbf{r}_b)$. A positive value of $H(\mathbf{r}_b)$ relates to a predominantly electrostatic interaction between the two atoms.

Since there is no bond critical point U−X′, we had to resort to calculating $H(\mathbf{r}_b)$ for each of the U-ring atom interactions (C and/or P) and averaging over the $H(\mathbf{r}_b)$ values of all U-ring atom interactions (i.e., sum over the five $H(\mathbf{r}_b)$ values and divide by five), an often applied procedure.[33,67] For some complexes, only m U-ring atom bond critical points could be found with $m < 5$. In these cases, we summed over the m $H(\mathbf{r}_b)$ values and divided by m. This protocol has to be kept in mind when comparing averaged $H(\mathbf{r}_b)$ with k^a(U−X′) values.[33]

https://doi.org/10.1021/acs.inorgchem.3c01761
Inorg. Chem. 2023, 62, 12510−12524

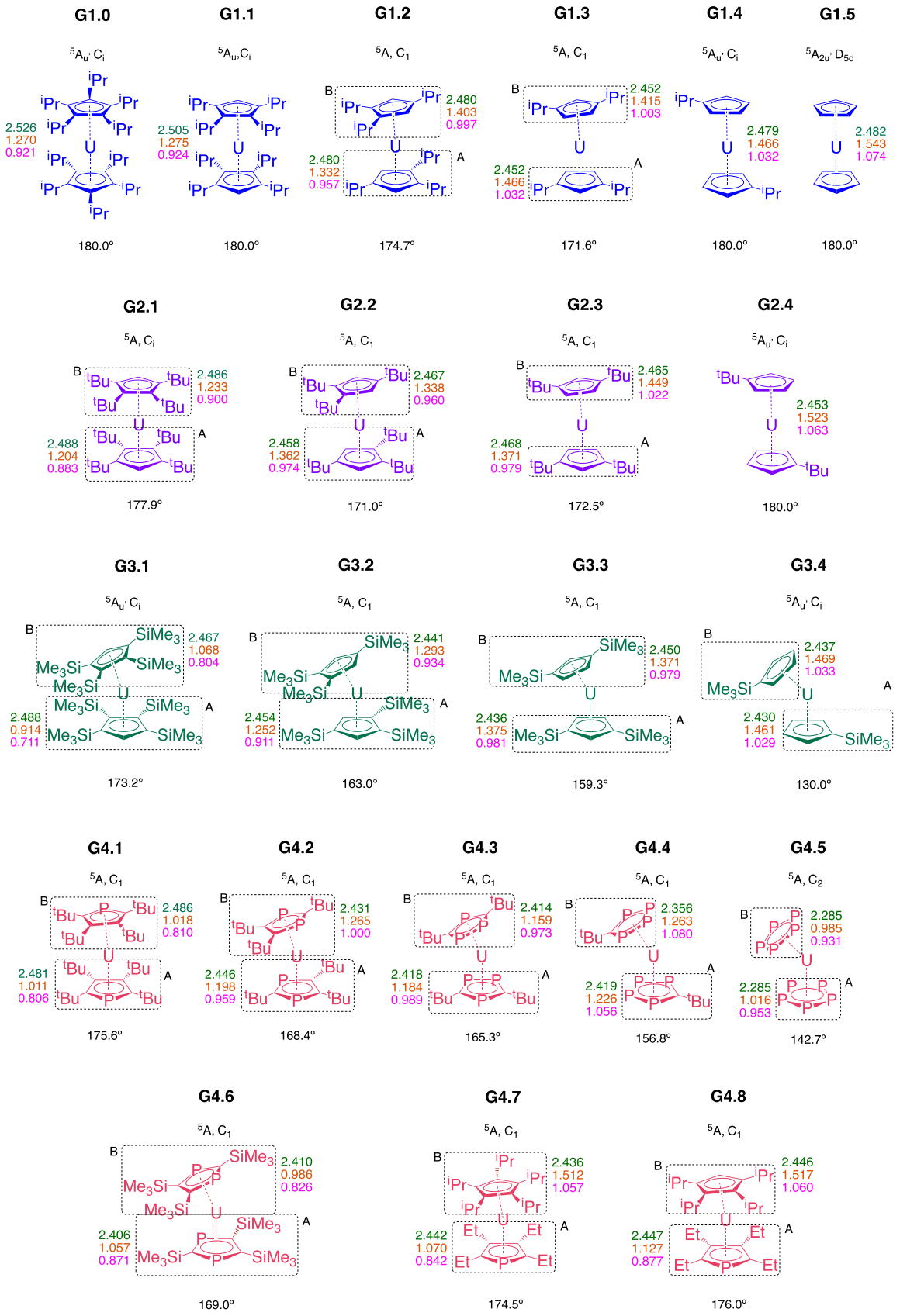

Figure 4. Summary of structural and LMA results. U-ring distances (green); k^a(U−X′) (orange), and BSO n (pink). Electronic term symbols, symmetry point groups, and X′−U−X′ angles are given as well as ring labels A and B. PBE0/NESCau/cc-pVDZ/SARC-DKH2(U) level of theory.

Potential shortcomings of this approach are discussed in more detail in the Results and Discussion section.

Computational Procedures. Geometry optimizations were performed for molecules displayed in Figure 2 at the

https://doi.org/10.1021/acs.inorgchem.3c01761
Inorg. Chem. 2023, 62, 12510−12524

Table 1. Summary of Geometric, Electronic, and Vibrational Data[a,b]

	U–X′ A				U–X′ B				X′–U–X′		U config.	ΔE_{gap}
	r	k^a(U–X′)	BSO n	$H(r_b)$	r	k^a(U–X′)	BSO n	$H(r_b)$	angle	k^a(X′–U–X′)		
G1.0	2.526	1.270	0.921	−1.42	2.526	1.270	0.921	−1.42	180.0	0.728	$5f^{2.8}6d^{1.0}7s^{0.6}$	1.920
G1.1	2.505	1.275	0.924	−1.93	2.505	1.275	0.924	−1.93	180.0	0.342	$5f^{2.1}6d^{2.0}7s^{0.5}$	1.755
G1.2	2.480	1.332	0.957	−1.88	2.480	1.403	0.997	−1.76	174.7	0.216	$5f^{2.5}6d^{1.5}7s^{0.6}$	1.909
G1.3	2.452	1.466	1.032	−2.18	2.452	1.415	1.003	−2.15	171.6	0.325	$5f^{2.4}6d^{1.8}7s^{0.5}$	2.121
G1.4	2.479	1.466	1.032	−1.73	2.479	1.466	1.032	−1.73	180.0	0.068	$5f^{2.8}6d^{1.0}7s^{0.7}$	1.900
G1.5	2.482	1.543	1.074	−1.62	2.482	1.543	1.074	−1.62	180.0	0.081	$5f^{2.8}6d^{1.0}7s^{0.7}$	1.915
G2.1	2.488	1.204	0.883	−3.31	2.486	1.233	0.900	−3.67	177.9	0.781	$5f^{2.6}6d^{1.5}7s^{0.3}$	2.170
G2.2	2.458	1.362	0.974	−2.21	2.467	1.338	0.960	−2.97	171.0	0.371	$5f^{2.6}6d^{1.4}7s^{0.4}$	2.156
G2.3	2.468	1.371	0.979	−2.28	2.465	1.449	1.022	−1.82	172.5	0.171	$5f^{2.6}6d^{1.5}7s^{0.5}$	2.126
G2.4	2.453	1.523	1.063	−2.05	2.453	1.523	1.063	−2.05	180.0	0.212	$5f^{2.1}6d^{2.4}7s^{0.4}$	1.599
G3.1	2.488	0.914	0.711	−3.72	2.467	1.068	0.804	−2.25	173.2	0.607	$5f^{2.6}6d^{1.4}7s^{0.4}$	2.098
G3.2	2.454	1.252	0.911	−2.07	2.441	1.293	0.934	−3.30	163.0	0.361	$5f^{2.5}6d^{1.7}7s^{0.4}$	2.140
G3.3	2.450	1.371	0.979	−2.11	2.436	1.375	0.981	−2.91	159.3	0.227	$5f^{2.6}6d^{1.5}7s^{0.4}$	2.117
G3.4	2.430	1.461	1.029	−2.95	2.437	1.469	1.033	−2.22	130.0	0.659	$5f^{2.6}6d^{1.3}7s^{0.7}$	2.192
G4.1	2.481	1.011	0.806	−3.46	2.486	1.018	0.810	−4.01	175.6	0.896	$5f^{2.6}6d^{1.7}7s^{0.2}$	
G4.2	2.446	1.198	0.959	−5.20	2.431	1.265	1.000	−4.05	168.4	0.514	$5f^{2.5}6d^{1.7}7s^{0.2}$	
G4.3	2.418	1.184	0.989	−5.27	2.414	1.159	0.973	−5.27	165.3	0.240	$5f^{2.2}6d^{2.1}7s^{0.3}$	
G4.4	2.419	1.226	1.056	−5.03	2.356	1.263	1.080	−4.70	156.8	0.747	$5f^{2.4}6d^{2.0}7s^{0.3}$	
G4.5	2.2845	1.016	0.953	−6.05	2.2846	0.985	0.931	−6.05	142.74	0.644	$5f^{2.1}6d^{2.6}7s^{0.3}$	
G4.6	2.410	0.986	0.826	−4.82	2.406	1.057	0.871	−4.82	169.0	0.319	$5f^{2.5}6d^{1.5}7s^{0.2}$	
G4.7	2.442	1.070	0.842	−2.86	2.436	1.512	1.057	−2.68	174.5	0.500	$5f^{2.5}6d^{1.6}7s^{0.4}$	
G4.8	2.447	1.127	0.877	−3.76	2.446	1.517	1.060	−2.91	176.0	0.299	$5f^{2.1}6d^{2.3}7s^{0.4}$	

[a]For an explanation about labels A and B, see the geometries section and Figure 4. [b]r values are displayed in Å; k^a(U–X′), in mdyn/Å; k^a(X′–U–X′), in mdynÅ /rad; angle in degrees and $H(r_b)$, in 10^{-2} Ha/Å^3. U config. refers to uranium electronic configuration. ΔE_{gap} is the HOMO–LUMO gap and it is given in eV. PBE0/NESCau/cc-pVTZ/jorge-DZP-DKH(U)//cc-pVDZ/SARC-DKH2(U) level of theory.

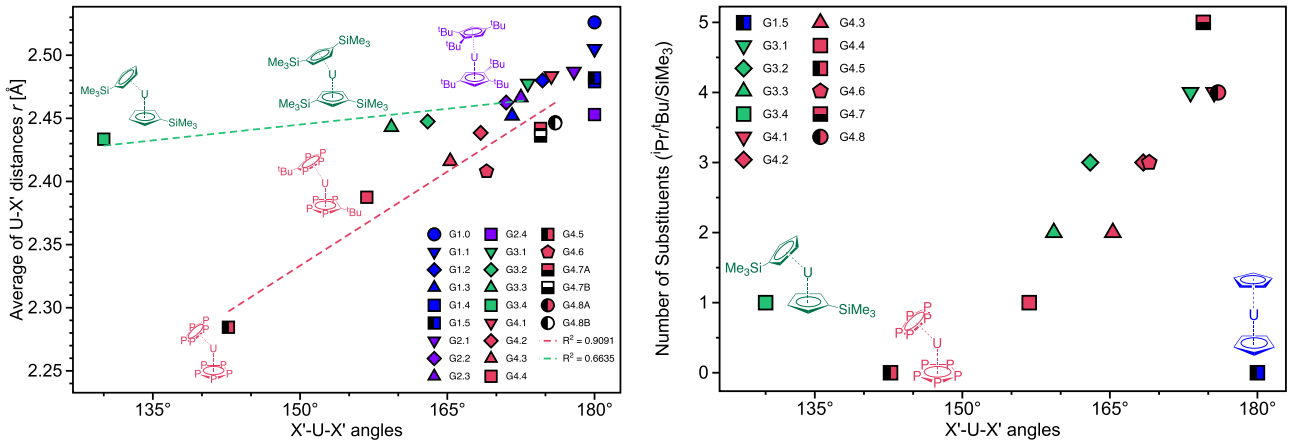

Figure 5. (a) Average of U–X′ distances r with respect to X′–U–X′ angles. For complexes **G4.7** and **G4.8**, the individual results of each ring are displayed instead of the average values: A: phosphacyclo-pentadienyl ring ligand, B: Cp ring (see Figure 4). (b) Correlation between X′–U–X′ angle and number of ring substituents for Group III and Group IV members. PBE0/NESCau/cc-pVDZ/SARC-DKH2(U) level of theory.

NESCau/ PBE0 level of the theory.[32,68−70] SARC-DKH2[71] basis functions were used for uranium, whereas cc-pVDZ[72,73] was employed for the remaining atoms (C, H, P, and Si).[74−76] An extensive prior study was performed on **G1.0** to validate our choice of basis set; for more information, see the Supporting Information. Calculations were performed under the unrestricted open-shell formalism and spin contamination was never greater than 0.022. Once the stationary geometry was found, the Hessian was calculated to confirm that the structure was indeed a minimum in the potential energy surface. NESCau/DFT calculations were performed using the COLOGNE2020 package[77] interfaced with Gaussian16.[78]

NBO analysis[79] was done to address U electronic configuration and its orbitals' nature. For this step in particular, we found that jorge-DZP-DKH[80] basis, for uranium, and cc-pVTZ,[72,73] for the remaining atoms, gave a better description. Calculations were performed at optimized geometries obtained with SARC-DKH2 and cc-pVDZ. NBO calculations were performed with the code NBO.[81] For LMA, the LmodeA code[82] was used. QTAIM calculations were done with the AIMALL package.[83]

https://doi.org/10.1021/acs.inorgchem.3c01761
Inorg. Chem. 2023, 62, 12510−12524

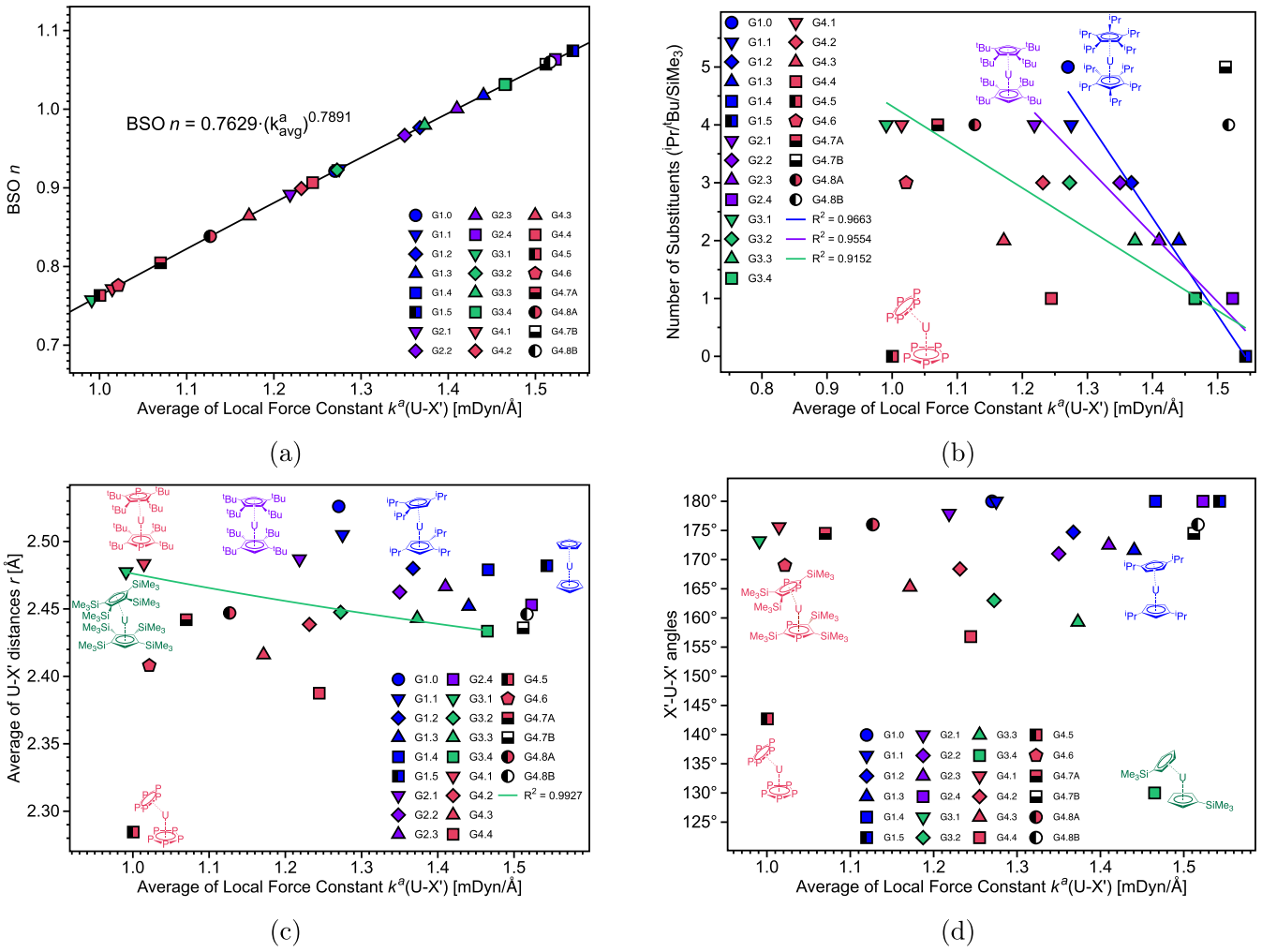

Figure 6. (a) Bond strength order curve for U-ring interactions. (b) Average of k^a(U−X′) vs the number of substituents on each ring. (c) Average of U−X′ distances vs averaged local force constant k^a(U−X′). For complexes **G4.7** and **G4.8**, the individual results of each ring are displayed instead of the average values: A: phosphacyclo-pentadienyl ring ligand, B: Cp ring (see Figure 4). (d) X′−U−X′ angles vs local force constant k^a(X′−U−X′). Calculated at PBE0/NESCau/cc-pVDZ/SARC-DKH2(U) level of theory.

RESULTS AND DISCUSSION

In this section, we report our findings on (i) the effects inducing bent U(II) sandwich complexes and (ii) what determines the strength of uranium-ring interactions exploring the effect of (i) removing bulky substituents (Group I and II); (ii) replacing electron-donating alkyl ring substituents with electron-withdrawing $SiMe_3$ ring substituents (Group III); and (iii) replacing one of the two ring ligands Cp carbon atoms with phosphorous atoms (Group IV). After presenting a summary of results, we focus in more detail on steric effects reflected in the geometries of Group I−Group IV members, followed by LMA, complemented with electron density and NBO analyses to capture electronic effects. Ring ligands are labeled as A and B as defined in Figure 4. Table 1 and Figure 4 present geometric, electronic, and vibrational data obtained in our work with both ring A and B data reported separately. In Figures 5−7, average results for rings A and B are presented for better readability, except for **G4.7** and **G4.8**. Optimized Cartesian coordinates for all complexes investigated in this work can be found in the Supporting Information.

Summary of Results. Figure 4 summarizes the essential findings of our study. The first important result is that systematically reducing the number of bulky ^{i}Pr ring substituents, **G1.0** to **G1.5** (Group I), and ^{t}Bu ring substituents, **G2.1** to **G2.4** (Group II), does not lead to a significant bending of the sandwich complexes, opposed to what one may assume. The most bent Group I member is **G1.3** with an X′−U−X′ angle of 171.6°, whereas **G1.4** with one ^{i}Pr group per Cp ring is linear. Interesting to note is that U−X′ distances show a different behavior, namely as expected, less crowded ligands lead to shorter U−X′ distances and stronger U−X′ interactions, ranging from 2.526 Å in **G1.0** to 2.479 Å in **G1.4** with corresponding BSO n values of 0.921 and 1.074, respectively. Group II shows the same trend. Reducing the number of bulky ^{t}Bu ring substituents does not significantly increase complex bending. The smallest X′−U−X′ angles of 171.0 and 172.5° are found for **G2.2** and **G2.3** (with three and two ^{t}Bu ring substituents per Cp ring, respectively). On the other hand, for Group I less crowded ring ligands lead to somewhat shorter U−X′ distances and stronger U−X′ interactions, ranging from 2.486 Å in **G2.1** to 2.453 Å in **G2.4** with corresponding BSO n values of 0.883 and 1.063, respectively. These findings suggest that steric effects do not play the only role in determining if the U(II) complex is bent. In contrast to Groups I and II, all Group III members with $SiMe_3$ instead of alkyl ring substituents are bent. Successive

https://doi.org/10.1021/acs.inorgchem.3c01761
Inorg. Chem. 2023, 62, 12510−12524

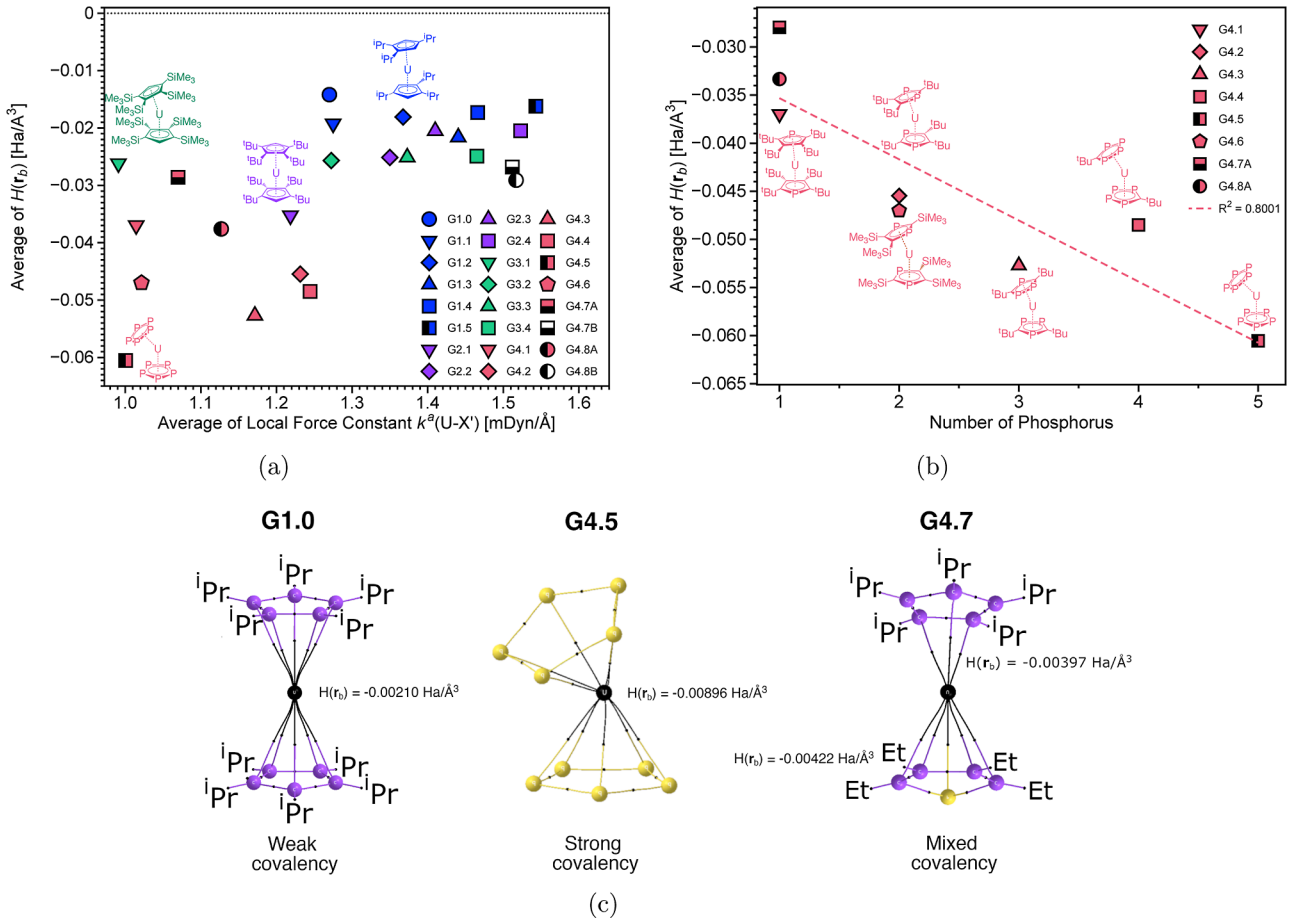

Figure 7. (a) Energy density $H(\mathbf{r}_b)$ averaged over U−C (U−P) bond critical points, with regard to the number of P atoms in the ring. For complexes **G4.7** and **G4.8**, only results pertaining to rings A, phosphacyclo-pentadienyl, are shown. (b) Energy density $H(\mathbf{r}_b)$ vs the average of local force constant k^a(U−X′). For complexes **G4.7** and **G4.8**, the individual results of each ring are displayed instead of the average values: A: phosphacyclo-pentadienyl ring ligand, B: Cp ring (see Figure 4). (c) Representatives with minor (**G1.0**), larger (**G4.5**), and mixed covalency (**G4.7**). Calculated at PBE0/NESCau/cc-pVDZ/SARC-DKH2(U) level of theory.

reduction of the $SiMe_3$ ring substituents leads to a decrease of the X′−U−X′ angle but only to somewhat shorter and stronger U−X′ bonds with U−X′ distances slightly decreasing from 2.467 Å in **G3.1** to 2.437 Å in **G3.4** and corresponding BSO n values increasing from 0.840 to 1.033, respectively. **G3.4** has 130°, the smallest X′−U−X′ angle of all complexes investigated in this work. This clearly shows that electronic effects play the most significant role for Group III, whereas Group IV is an example of the interplay of steric and electronic effects. Successively replacing carbon Cp atoms with phosphorous atoms while reducing ^{t}Bu ring substituents leads to bent complexes as shown for the series **G4.1**−**G4.5**. Interesting to note is that **G4.5** with all carbon ring atoms being replaced by phosphorous atoms and all ^{t}Bu ring substituents with hydrogen is with an X′−U−X′ angle of 142.7°, the second most bent U(II) sandwich complex investigated in this work. It also has the shorted U−X′ distance (2.285 Å) of all complexes, although this U−X′ bond is not the strongest. This is another exception to the rule that the shortest bond should also be the strongest.[84,85] Interesting to note is that replacing ^{t}Bu with $SiMe_3$ ring substituents do not significantly increase bending, as reflected by the X′−U−X′ angles of 168.4 and 169.0° of **G4.2** and **G4.6**, respectively, suggesting that effects resulting from replacement of Cp carbon atoms and changing ring substituents are not necessarily additive. Furthermore, as the results for **G4.1**, **G4.6**, and **G4.7** show, at least two Cp ring carbon atoms have to be replaced with phosphorous to produce a notable effect on complex bending.

Structural and Steric Effects. Figure 5 illustrates in more detail the relationship between the U−X′ distance and the X′−U−X′ angle. As already suggested, there is no correlation between these two quantities for Group I and Group II members. However, for Groups III and IV, we observed that bent complexes tend to have shorter U−X′ distances. As reflected by the R^2 value of 0.909, for Group IV members this tendency is more pronounced, i.e., successive replacement of the carbon Cp ring atoms with phosphorous decrease both X′−U−X′ angle and U-ring distance, as shown in Figure 5a. Interesting to note is that **G4.5** with two *cyclo*-P_5 ring ligands has the smallest Group IV X′−U−X′ angle, whereas removing all $SiMe_3$ ring substituents in Group III leads to the linear **G1.5** complex as shown in Figure 5b.

In summary, complex bending cannot entirely be attributed to a reduction of steric repulsion, the electronic structure of the U(II) metallocene has to be changed too, as demonstrated by the effect of $SiMe_3$ ring substituents or by the introduction of phosphacyclo-pentadienyl ring ligands.

Electronic Effects and Their Interplay with Steric Effects. To elucidate these electronic effects and their

https://doi.org/10.1021/acs.inorgchem.3c01761
Inorg. Chem. 2023, 62, 12510−12524

interplay with the steric effects, in this section local mode force constants $k^a(U-X')$ and corresponding BSO n values are presented and compared with U−X′ distances and X′−U−X′ angles. This is followed by a QTAIM analysis, first focusing on the covalent character of the U-ring interaction and then providing further insights via the Laplacian of $\rho(\mathbf{r})$. Finally, the NBO analysis addresses the question of 5f orbital occupation in these complexes.

The local mode force constant $k^a(U-X')$ (defined in Figure 3) is the perfect tool for assessing the individual strength of the U-ring ligand interaction and comparing the U-ring ligand strength across the four groups. Figure 6a shows BSO n as a function of $k^a(U-X')$, derived via eq 19. The BSO n values range from 0.75 (**G3.1**) to 1.08 (**G1.5**) identifying the U-ring interactions of all complexes investigated in this work as single bonds, in accordance with the valence of Cp and phosphacyclo-pentadienyl $C_{(5-x)}P_x$ (x = 1···5) ring ligands[11] and the U(II) valence. The phosphacyclo-pentadienyl ring ligand interactions of Group IV complexes fall into the lower BSO range; Group I−III U-ring interactions, including the U-Cp-ring interactions of **G4.7** and **G4.7**, fall into the higher BSO range, with the exception of **G3.1**.

Stronger U-ring interactions, characterized by the higher values of $k^a(U-X')$, emerge for Groups I and II. Group III exhibits intermediate results for $k^a(U-X')$, while the incorporation of phosphorus in the Cp ring ligands weakens U-ring interaction (see Figure 6b). Among Groups I−III, the successive removal of substituents increases $k^a(U-X')$, with its maximum value arising on the non-substituted **G1.5** (see Figure 6b). The strong interaction found for **G1.5** compares well with the strength of Fe-ring interactions found for ferrocene and ferrocene analogs.[33,52] The rate of increase on $k^a(U-X')$ is different in each group, as can be seen in the linear regression curves in Figure 6b. From the slopes, one perceives the pronounced weakening effect the successive inclusion of the electron-withdrawing $SiMe_3$[23] exerts on U-ring interactions, when compared to the alkyl substituents. In contrast to Groups I−III, complexes with phosphacyclo-pentadienyl ring ligands do not display a correlation between $k^a(U-X')$ and the number of substituents, as can be perceived by the scattered pattern exhibited by Group IV. Uranium-ring interaction in **G4.6** with $SiMe_3$ ring substituents is weaker than in **G4.2**, which contains the same number of ^{t}Bu groups, suggesting that the weakening effect brought on by $SiMe_3$ and the incorporation of P into the ring is additive. The lowest local force constants shown by Group IV have been previously observed in further metallocenes featuring phosphacyclo-pentadienyl rings.[11,52] **G4.5**, with *cyclo*-P_5 rings, displays an extreme result, as it has the weakest U-ring interaction.

Figure 6c displays the relationship between U-ring distances r and local force constants $k^a(U-X')$. There is no direct correlation between these two quantities for Groups I, II, and IV, only a weak trend that stronger interactions tend to have smaller U-ring distances r, where **G4.5** is a clear outlier. In contrast, Group III exhibits a Badger power relationship between r and $k^a(U-X')$ with R^2 = 0.993 comparable to what we observed for actinide metallocenes.[33] **G4.7** and **G4.8** illustrate the distinct effects of Cp and phosphacyclo-pentadienyl ligands on U-ring interactions, synchronized in one complex. Although in these complexes U-ring distances r are nearly identical for both ring ligands, their $k^a(U-X')$, reflecting their different electronic structure, are considerably distinct, with phosphacyclo-pentadienyl rings being clustered with the remainder of Group IV and Cp, close to Group I.

The relationship between X′−U−X′ angles and $k^a(U-X')$ force constants is inspected in Figure 6d focusing on the question if stronger U-ring interactions lead to bent complexes. The interplay between electronic and steric effects is illuminated from the local vibrational mode point of view. As reflected by Figure 6d, there is no direct correlation between these two quantities, opposing previous suggestions that electronic effects would act in conjunction with the steric repulsion which prevents a greater bend to define the complex geometry.[22] Most points cluster in the range of 165−180° with Group I and II members occupying the range of 170−180°, independent of the number of bulky Cp ring substitutes. Within Group III, there is a weak trend that the complex bends as the U-ring interactions strengthen, going in line with the reduction of bulky ring substituents. The most bent complex, **G3.4** is also the strongest in the Group III series and the one with only one $SiMe_3$ substituent per Cp ring. Group IV members follow the same trend, with one distinct outlier, **G4.5**. Although it has the second largest X′−U−X′ angle found in this work and pure *cyclo*-P_5 ring ligands, i.e., no bulky groups, it has one of the weakest U-ring interactions found. Another interesting Group IV result concerns the complexes featuring mixed rings, **G4.7** and **G4.8**. As observed for the U-ring distances r, we find that the Cp ring data points in the Group I region, whereas phosphacyclo-pentadienyl ring data can be found in the Group IV area, illustrating that phosphacyclo-pentadienyl ring ligand and Cp ring ligand prevail their distinct character even if they appear as ligands in the same complex.

In summary, LMA reveals how different ligands tune the strength associated with U-ring interactions and how the interaction strength coordinates with complex bending and ring substituent effects. Complexes containing mixed ring ligands exhibit distinct $k^a(U-X')$ constants being based on their different electronic nature. This opens the possibility to include strong and weak U-ring interactions in the same complex, an interesting aspect for catalyst design.

The topological analysis of the electronic density was employed as supplementary machinery in conjunction with LMA to further characterize U-ring interactions. We used the energy density $H(\mathbf{r}_b)$ as a tool to assess the covalency of the U-ring interactions, according to the procedure described above. $H(\mathbf{r}_b)$ results, averaged over each U-ring atom bond critical points, are displayed in Table 1. Overall, we observed small covalent contributions (i.e., slightly negative $H(\mathbf{r}_b)$ values) for all U-ring interactions investigated in this work, in agreement with the past and current literature data on uranocenes in particular[24,67] and on actinides metallocenes in general,[86,87] both featuring carbon U-ring ligands. Cp U-ring ligands with alkyl substituents (Groups I and II) tend to exhibit a smaller covalent character compared to other uranium ligand interactions, such as U−CO.[67] Introduction of $SiMe_3$ Cp ring substituents increases covalency to some extent. The $SiMe_3$ group has been previously pointed out as more prone to induce U-ring covalency than CH_3 ring substituents.[24] In this regard, Groups I and II results can be considered as natural extensions to ^{i}Pr and ^{t}Bu groups. A different scenario arises for phosphacyclo-pentadienyl ring ligands displaying a more substantial increase in U-ring covalency. As an example, **G4.5** with pure *cyclo*-P_5 ring ligands has an $H(\mathbf{r}_b)$ value of -6.05×10^{-2} Ha/Å^3 for all U−P interactions, which is 3.7

https://doi.org/10.1021/acs.inorgchem.3c01761
Inorg. Chem. 2023, 62, 12510−12524

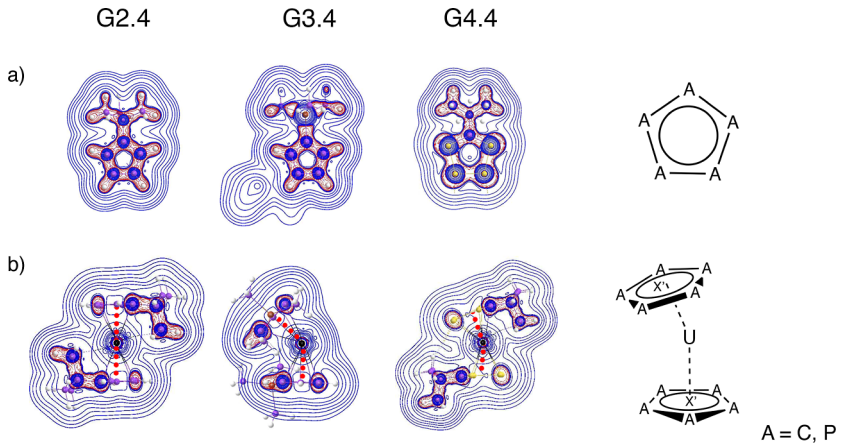

Figure 8. (a) Laplacian of the electronic density in the ring plane for **G2.4**, **G3.4**, and **G4.4**. (b) Laplacian of the electronic density in the plane containing both ring midpoints X′ sandwiched by uranium for **G2.4**, **G3.4**, and **G4.4**. Red dashed lines account for negative $\nabla^2(\rho(\mathbf{r}))$ values (charge concentration) and for negative values and blue solid lines for positive $\nabla^2(\rho(\mathbf{r}))$ values (charge depletion). Obtained with a resolution of 0.01. The dotted red lines in the bottom part visualize the location of X′−U−X′. Calculated at PBE0/NESCau/cc-pVDZ/SARC-DKH2(U) level of theory.

times greater than that found for the Cp ring ligand analog **G1.5**.

Figure 7a exemplifies these results; there are two major groups, complexes of smaller covalency for complexes containing Cp rings either with alkyl substituents (Groups I and II) or $SiMe_3$ substituents and complexes with larger covalency for Group IV members with two phosphacyclo-pentadienyl ring ligands. Group (IV) members **G4.7** and **G4.8** with one Cp ring ligand and one phosphacyclo-pentadienyl ligand display smaller covalency for the Cp ring and larger covalency for the phosphacyclo-pentadienyl ring.

As obvious from Figure 7a, there is no direct correlation between $H(\mathbf{r}_b)$ and k^a(U−X′). As discussed above, k^a(U−X′) is defined between the U atom and the ring center and as such captures all electronic effects of the U-ring ligand interaction. Averaging over the $H(\mathbf{r}_b)$ values of the U-ring atom bonds cannot represent U-ring interactions in the same precise way, in particular as $H(\mathbf{r}_b)$ values may fluctuate for each U-ring atom bond depending on the U-ring atom bond length and the type of substituent. However, there is a trend for Group IV members that with increasing number of P ring atoms, the covalency increases, as depicted in Figure 7b. Figure 7c displays the network of U-ring atom bonds, for a complex with weak covalency (**G1.0**), for a complex with stronger covalency (**G4.5**), and for a complex with mixed ring ligands (**G4.7**). The covalency of the phosphacyclo-pentadienyl ring in **G4.7**, $H(\mathbf{r}_b) = -2.86 \times 10^{-2}$ Ha/Å^3, is slightly larger than that of the Cp ring, $H(\mathbf{r}_b) = -2.68 \times 10^{-3}$ Ha/Å^3; however the covalency of such Cp ring is greater than that found for **G1.0**, $H(\mathbf{r}_b) = -1.42 \times 10^{-3}$ Ha/Å^3, which may be caused by the fact that only three U-Cp atom bond paths were found. This again shows that a direct comparison of $H(\mathbf{r}_b)$ and k^a(U−X′) has to be made with care.

To gain further insight into the electronic structure specifics of the U-ring interaction, we explored higher derivatives of the electron density $\rho(\mathbf{r})$, namely the gradient vector field $\nabla(\rho(\mathbf{r}))$, providing the network of bond paths and the Laplacian of the electronic density, $\nabla^2(\rho(\mathbf{r}))$, disclosing local regions of charge concentration (negative values of $\nabla^2(\rho(\mathbf{r}))$) and depletion (positive values of $\nabla^2(\rho(\mathbf{r}))$).[66,88] This is illustrated for complexes **G2.4**, **G3.4**, and **G4.4** shown in Figure 8. Similar contour maps for the remainder of the complexes are provided in the Supporting Information. The Laplacian maps were generated (i) in a plane containing one of the ring ligands (Figure 8a) and (ii) in a plane containing both ring midpoints X′ sandwiched by the uranium atom (Figure 8b). As an overall picture of the planes encompassed by the ring ligands, one perceives that Cp rings with alkyl substituents exhibit a somewhat uniform pattern on the electronic density distribution (see **G2.4** in Figure 8a). Replacement of the ^{t}Bu ring substituent by $SiMe_3$ perturbs the distribution of $\nabla^2(\rho(\mathbf{r}))$, where a region of charge depletion arises in the vicinity of silicon provoking an abrupt change in the $\nabla^2(\rho(\mathbf{r}))$ signal along the Cp ring C−Si bond path. Such discontinuity breaks the charge flux between the ring and substituent previously observed in **G2.4**, reflecting the electron-withdrawing character of the $SiMe_3$ ring substituent,[24] when compared to alkyl ring substituents. In contrast, the incorporation of P increases regions of charge concentration, as can be seen in Figure 8a in **G4.4**, suggesting the higher electron donor character of phosphacyclo-pentadienyl rings, when compared to the Cp ring. It should be mentioned that the $\nabla^2(\rho(\mathbf{r}))$ pattern for our Group IV molecules is similar to the ones exhibited by transition-metal metallocenes featuring phosphacyclo-pentadienyl rings.[27] Contour maps displayed in Figure 8b disclose the electronic profile along the U-ring interaction, where charge depletion regions predominate. Such a finding corroborates the weak covalent character of U-ring interactions, as previously discussed. In essence, the introduction of novel chemical species into the Cp ring ligand with alkyl substituents altered the electronic environment in the complex, culminating in a nonuniform electronic distribution. This suggests that a higher reactivity can be associated with **G3.4** and **G4.4**, while **G2.4** would exhibit a more inert profile.

To accomplish our investigation of electronic effects associated with the geometry of U(II) metallocenes, we evaluated uranium electronic configuration in Groups I−III through NBO analysis. The electronic configuration, particularly the role of f electrons in the molecular arrangement, has been previously investigated for U(III), U(IV), and U(V) complexes through molecular orbital analysis.[89] We focused our attention on uranium valence, considering particularly the participation of 5f electrons in the chemical bonding. Our

https://doi.org/10.1021/acs.inorgchem.3c01761
Inorg. Chem. 2023, 62, 12510−12524

NBO results indicate that U electronic configuration ranges from $5f^{2.8}6d^{1.0}7s^{0.7}$ to $5f^{2.1}6d^{2.4}7s^{0.4}$, confirming the existence of 4 unpaired electrons in singly occupied molecular orbitals (SOMOs) and the formal oxidation state of +2. Given the range of 5f occupation and the fact that linear U(II) metallocenes display 3 electrons in 5f orbitals,[7,8] we initially investigated whether the absolute 5f occupancy would display any relationship with regard to the X′−U−X′ angle. As can be seen from Figure 9, there is no direct correlation between

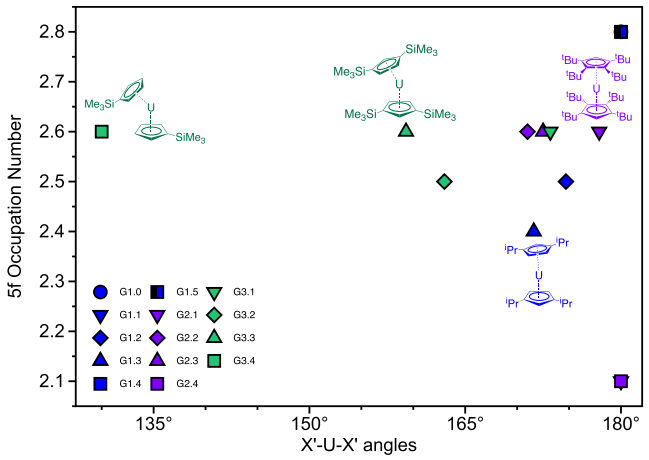

Figure 9. 5f occupation number vs X′−U−X′ angles. Calculated at PBE0/NESCau/cc-pVDZ/SARC-DKH2(U)//cc-pVDZ/SARC-DKH2(U) level of theory.

those two quantities, suggesting that further investigation into the existence of hybridized orbitals should be considered. Similar to **G1.0**, further U(II) metallocenes displayed at least one hybridized orbital. Nonetheless, in addition to the s/d orbital mixture, hybridizations containing f character arose, in particular on complexes of bent structure.

Linear representatives in Groups I and II exhibited voluminous orbitals featuring s/d hybridization (see Figure 10a, **G1.4**), in line with previous findings on linear U(II) metallocenes.[7,8] Such a large spatial extent has been previously associated with the absence of a bend. Additionally, one can correlate the higher sphericity and non-directional character with the previous findings, where we associated small covalency and lower reactivity with U(II) metallocenes featuring Cp ring ligands with alkyl substituents. The remainder of the three SOMOs in linear structures are not hybridized, exhibiting pure f character. The exceptions are **G1.1** and **G2.4**, which exhibited one NBO of pure d content and two of f character. Orbital plots for the remainder of the structures are available as Supporting Information. **G2.1** exhibits SOMOs with minor hybridization, where f and d contents are greater than 90% (see Figure 10a, **G2.1**). The lack of rigorousness in those orbitals' purity reflects on their small directionality, which can be associated with the minor bend manifested by **G2.1** (X′−U−X′ equals 177°). Furthermore, small covalency arose on this complex, as it was located at a bonding orbital containing 71% of U contribution. This finding agrees with the more negative energy density result displayed by **G2.1** (see Figure 7b).

Hybridized orbitals with f content arose in Group III and bent structures from Groups I and II, as can be seen in Figure 10b. Similar to the s/d mixture, these orbitals exhibit a large extent, nonetheless the previously observed uniform shape is

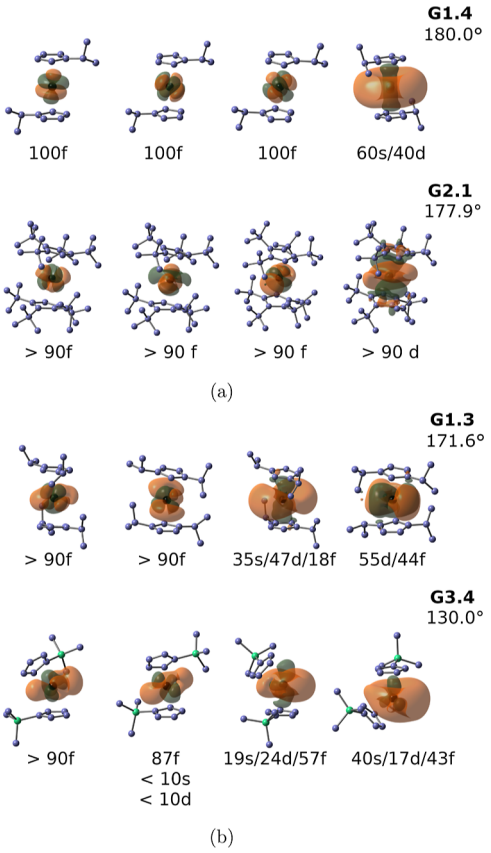

Figure 10. (a) NBO plots for **G1.4** and **G2.1**. (b) NBO plots for **G1.3** and **G3.4**. Purple: carbon; black: uranium; Green: silicon. Hydrogens were omitted for clarity. Calculated at 0.05 isovalue. Calculated at PBE0/NESCau/cc-pVTZ/jorge-DZP-DKH(U)//cc-pVDZ/SARC-DKH2(U) level of theory.

lacking. The inclusion of f orbitals into the hybridization brings on directionality,[90] which can be related to the nonuniform electron density distribution previously observed. From Figure 10b, one perceives that SOMOs from **G3.4** are highly asymmetric, which correlates with the greater bend observed on this molecule and the more pronounced covalent character when compared to the alkyl substituted complexes, Groups I and II (see Figure 7b). In contrast, the shape of SOMOs in **G1.3** has higher uniformity, reflecting the minor bend exhibited by the complex. In Maynadié et al.'s[89] study, the participation of f electrons and the directionality of hybridized orbitals have been associated with the bend exhibited by uranium metallocenes.

Complementing the conjecture of s/d hybridization as the main aspect involved in the linear arrangement exhibited by a U(II) metallocene, we suggest the participation of f orbitals in such mixing as a factor that brings bend to the structure. The higher the asymmetry of the hybrid orbitals' shape, the more directional the U-ring interaction would be, increasing the covalent character. Henceforth, NBO results agree with the previous QTAIM analysis.

CONCLUSIONS

This study performed all-electron relativistic calculations, using the NESCau Hamiltonian, on 22 U(II) metallocenes, containing up to 117 atoms. Electronic aspects of U-ring interactions were extensively investigated through local vibrational mode analysis, topological analysis of the energy

https://doi.org/10.1021/acs.inorgchem.3c01761
Inorg. Chem. 2023, 62, 12510−12524

and electronic densities, and natural bonding orbital analysis. Our results shed light on important aspects of U(II) metallocenes properties, in particular on what concerns the structure and nature of their chemical bonding. The major findings of this study can be summarized as:

- Complexes featuring alkyl ring substituents tend to be either linear or exhibit minor bends. **G1.4** and **G2.4** with one ^{i}Pr and ^{t}Bu ring substituent per ring, respectively, and the non-substituted **G1.5** are linear, reflecting that steric hindrance is not the major aspect to be considered with regard to the linearity of U(II) metallocenes. In contrast, the $SiMe_3$ ring substituent and phosphacyclo-pentadienyl ring ligands favor bent arrangements. In particular, optimized structures for **G3.4** (Cp ring ligands with one $SiMe_3$ ring substituent per ring) and **G4.5** (P_5 ring ligand) are highly bent, reflecting the pronounced effect provided by the change on the electronic structure in conjunction with the lack of steric effects.
- BSO *n* provided a chemical transcription to LMA results, indicating that U-ring interactions considered in this study are of the single bond type, despite the broad range of local force constant results. LMA demonstrates that alkyl substituents have stronger interactions with uranium, while phosphacyclo-pentadienyl ring ligands display weaker interactions. Electron-withdrawing groups, such as the $SiMe_3$ ring substituent, display intermediate $k^a(U-X')$ values. For a given ring substituent on the Cp ring ligand, (i) the strength associated with U-ring interaction decreases with the addition of ring substituent groups and (ii) the bond distance weakly correlates with the local force constant with a Badger-like relationship.
- QTAIM analysis, through the Cremer−Kraka criterion, quantified the covalency associated with U-ring interactions. The smaller covalent character observed on Cp ring ligands with alkyl ring substituents might be associated with their stronger U-ring interactions. Nonetheless, a formal correlation between energy density and LMA results cannot be established because of the different protocols utilized for the assessment of $k^a(U-X')$ and $H(\mathbf{r}_b)$. The inclusion of P atoms into the ring increases covalent contributions. Laplacian maps of the electronic density in the ring plane illustrated how the electronic environment is altered as $SiMe_3$ ring substituents and phosphacyclo-pentadienyl ring ligands are included. The electronic profile on the plane encompassed by uranium and each ring midpoint X′ validated the weaker covalency that we associated with U-ring interactions.
- NBO analysis on novel linear U(II) metallocenes demonstrated the existence of s/d hybridization, in line with previous observations on linear U(II) metallocenes. Such hybrid orbitals are of higher sphericity and display a large spatial extent. Furthermore, bent molecules exhibit a novel type of hybridization, with f orbitals contributions. These mixed orbitals have a nonuniform shape and can be associated with higher covalency and the bend of the complex.

In essence, the different quantum chemical tools applied in this work perfectly complement each other providing a holistic picture of the structural and electronic features of these U(II) metallocenes including structural and electronic changes driven by the inclusion of $SiMe_3$ ring substituents and/or phosphacyclo-pentadienyl ring ligands. As our results reveal, the bent structure of a U(II) metallocene, such as **G1.0**, can be induced by (i) modifying Cp ring substituents, such as the introduction of the electron-withdrawing ring substituent $SiMe_3$, or (ii) incorporating P into the ring. The same elements can be utilized in tuning U-ring interaction strength and covalency, allowing for the design of U(II) metallocenes with specific physicochemical properties and higher reactivity.

■ ASSOCIATED CONTENT

Supporting Information

The Supporting Information is available free of charge at https://pubs.acs.org/doi/10.1021/acs.inorgchem.3c01761.

Detailed descriptions of computational time, choice of basis sets and plots of NBO orbitals, Laplacian maps of the electronic density, and optimized coordinates (PDF)

■ AUTHOR INFORMATION

Corresponding Author

Elfi Kraka − *Computational and Theoretical Chemistry Group (CATCO), Department of Chemistry, Southern Methodist University, Dallas, Texas 75275-0314, United States;* orcid.org/0000-0002-9658-5626; Phone: +1 214-768-1609; Email: ekraka@smu.edu

Authors

Bárbara M. T. C. Peluzo − *Computational and Theoretical Chemistry Group (CATCO), Department of Chemistry, Southern Methodist University, Dallas, Texas 75275-0314, United States*

Małgorzata Z. Makoś − *Computational and Theoretical Chemistry Group (CATCO), Department of Chemistry, Southern Methodist University, Dallas, Texas 75275-0314, United States; Chemical Sciences Division, Oak Ridge National Laboratory, Oak Ridge, Tennessee 37830, United States*

Renaldo T. Moura, Jr. − *Department of Chemistry and Physics, Center of Agrarian Sciences, Federal University of Paraíba, Areia 58397-000 Paraíba, Brazil; Computational and Theoretical Chemistry Group (CATCO), Department of Chemistry, Southern Methodist University, Dallas, Texas 75275-0314, United States;* orcid.org/0000-0002-8151-1640

Marek Freindorf − *Computational and Theoretical Chemistry Group (CATCO), Department of Chemistry, Southern Methodist University, Dallas, Texas 75275-0314, United States*

Complete contact information is available at: https://pubs.acs.org/10.1021/acs.inorgchem.3c01761

Notes

The authors declare no competing financial interest.

■ ACKNOWLEDGMENTS

This work was financially supported by the National Science Foundation, grant number CHE 2102461. We thank SMU for the computational resources and CATCO members for all fruitful discussions. B.M.T.C.P. thanks Filippo Bodo, Juliana Antonio, and Mateus Quintano for the valuable suggestions.

REFERENCES

(1) Streitwieser, A.; Mueller-Westerhoff, U. Bis (Cyclooctatetraenyl) Uranium (Uranocene). A New Class of Sandwich Complexes that Utilize Atomic f Orbitals. *J. Am. Chem. Soc.* **1968**, *90*, 7364.

(2) Kahan, R. J.; Farnaby, J. H.; Tsoureas, N.; Cloke, F. G. N.; Hitchcock, P. B.; Coles, M. P.; Roe, S. M.; Wilson, C. Sterically Encumbered Mixed Sandwich Compounds of Uranium (III): Synthesis and Reactivity with Small Molecules. *J. Organomet. Chem.* **2018**, *857*, 110−122.

(3) Tsoureas, N.; Mansikkamäki, A.; Layfield, R. A. Synthesis, Bonding Properties and Ether Activation Reactivity of Cyclobutadienyl-ligated Hybrid Uranocenes. *Chem* **2021**, *12*, 2948−2954.

(4) Wedal, J. C.; Murillo, J.; Ziller, J. W.; Scott, B. L.; Gaunt, A. J.; Evans, W. J. Synthesis of Trimethyltriazacyclohexane (Me_3tach) Sandwich Complexes of Uranium, Neptunium, and Plutonium Triiodides:$(Me_3tach)_2AnI_3$. *Inorg. Chem.* **2023**, *62*, 5897−5905.

(5) MacDonald, M. R.; Fieser, M. E.; Bates, J. E.; Ziller, J. W.; Furche, F.; Evans, W. J. Identification of the +2 Oxidation State for Uranium in a Crystalline Molecular Complex,[K(2.2.2-Cryptand)] $[(C_5H_4SiMe_3)_3U]$. *J. Am. Chem. Soc.* **2013**, *135*, 13310−13313.

(6) Tsoureas, N.; Mansikkamäki, A.; Layfield, R. A. Uranium(IV) Cyclobutadienyl Sandwich Compounds: Synthesis, Structure and Chemical Bonding. *Chem. Commun.* **2020**, *56*, 944−947.

(7) Guo, F.-S.; Tsoureas, N.; Huang, G.-Z.; Tong, M.-L.; Mansikkamäki, A.; Layfield, R. A. Isolation of a Perfectly Linear Uranium (II) Metallocene. *Angew. Chem., Int. Ed.* **2020**, *59*, 2299−2303.

(8) Yu, J. M.; Furche, F. Theoretical Study of Divalent Bis (Pentaisopropylcyclopentadienyl) Actinocenes. *Inorg. Chem.* **2019**, *58*, 16004−16010.

(9) La Pierre, H. S.; Scheurer, A.; Heinemann, F. W.; Hieringer, W.; Meyer, K. Synthesis and Characterization of a Uranium(II) Monoarene Complex Supported by δ Backbonding. *Angew. Chem., Int. Ed.* **2014**, *53*, 7158−7162.

(10) Barluzzi, L.; Giblin, S. R.; Mansikkamäki, A.; Layfield, R. A. Identification of Oxidation State +1 in a Molecular Uranium Complex. *J. Am. Chem. Soc.* **2022**, *144*, 18229−18233.

(11) Mathey, F. The Chemistry of Phospha-and Polyphosphacyclopentadienide Anions. *Coord. Chem. Rev.* **1994**, *137*, 1−52.

(12) Nief, F.; Mathey, F. A New Application of the Tetramethylphospholyl (η^5-C_4Me_4P) π-ligand. Synthesis of η^5-tetramethylphospholyl Complexes of Yttrium and Lutetium. *J. Chem. Soc., Chem. Commun.* **1989**, 800−801.

(13) Nief, F.; Ricard, L.; Mathey, F. Phospholyl (phosphacyclopentadienyl) and Arsolyl (arsacyclopentadienyl) Complexes of Ytterbium (II) and Samarium (II). Synthetic, Structural and Multinuclear (^{31}P and ^{171}Yb) NMR Studies. *Polyhedron* **1993**, *12*, 19−26.

(14) Baudry, D.; Ephritikhine, M.; Nief, F.; Ricard, L.; Mathey, F. Synthesis of Phospholyltetrahydroboratouranium Complexes. Crystal Structure of $[(\eta^5\text{-}C_4Me_4P)_2U(BH_4)_2]$. *Angew. Chem., Int. Ed.* **1990**, *29*, 1485−1486.

(15) Gradoz, P.; Boisson, C.; Baudry, D.; Lance, M.; Nierlich, M.; Vigner, J.; Ephritikhine, M. Synthesis, crystal structure and some derivatives of the chlorotris(tetramethylphospholyl)uranium. *J. Chem. Soc., Chem. Commun.* **1992**, 1720.

(16) Gradoz, P.; Baudry, D.; Ephritikhine, M.; Nief, F.; Mathey, F. Phospholyluranium Complexes. *J. Chem. Soc., Dalton Trans.* **1992**, 3047.

(17) Wang, Z.-C.; Qiao, L.; Sun, Z.-M.; Scheer, M. Inorganic Ferrocene Analogue $[Fe(P_4)_2]^{2-}$. *J. Am. Chem. Soc.* **2022**, *144*, 6698−6702.

(18) Straub, M. D.; Ouellette, E. T.; Boreen, M. A.; Britt, R. D.; Chakarawet, K.; Douair, I.; Gould, C. A.; Maron, L.; DelRosal, I.; Villarreal, D.; et al. A Uranium(II) Arene Complex That Acts as a Uranium(I) Synthon. *J. Am. Chem. Soc.* **2021**, *143*, 19748−19760.

(19) Tsoureas, N.; Castro, L.; Kilpatrick, A. F.; Cloke, F. G. N.; Maron, L. Controlling Selectivity in the Reductive Activation of CO_2 by Mixed Sandwich Uranium (III) Complexes. *Chem* **2014**, *5*, 3777−3788.

(20) Berthet, J.-C.; Thuéry, P.; Ephritikhine, M. Bending of "Uranocene"$((\eta^8\text{-}C_8H_8)_2U)$: Synthesis and Crystal Structure of the Cyanido Complex $[(\eta^8\text{-}C_8H_8)_2U(CN)][NEt_4]$. *Organometallics* **2008**, *27*, 1664−1666.

(21) Tsoureas, N.; Summerscales, O. T.; Cloke, F. G. N.; Roe, S. M. Steric Effects in the Reductive Coupling of CO by Mixed-sandwich Uranium (III) Complexes. *Organometallics* **2013**, *32*, 1353−1362.

(22) Maynadié, J.; Berthet, J.-C.; Thuéry, P.; Ephritikhine, M. An Unprecedented Type of Linear Metallocene With an f-element. *J. Am. Chem. Soc.* **2006**, *128*, 1082−1083.

(23) Zachmanoglou, C. E.; Docrat, A.; Bridgewater, B. M.; Parkin, G.; Brandow, C. G.; Bercaw, J. E.; Jardine, C. N.; Lyall, M.; Green, J. C.; Keister, J. B. The Electronic Influence of Ring Substituents and Ansa Bridges in Zirconocene Complexes as Probed by Infrared Spectroscopic, Electrochemical, and Computational Studies. *J. Am. Chem. Soc.* **2002**, *124*, 9525−9546.

(24) Su, D.-M.; Cai, H.-X.; Zheng, X.-J.; Niu, S.; Pan, Q.-J. Theoretical design and exploration of low-valent uranium metallocenes via manipulating cyclopentadienyl substituent. *Comput. Theor. Chem.* **2021**, *1195*, 113107.

(25) Caliman, V. The Wide Synthetic Versatility of Five Membered Rings Containing Phosphorus. *Quim. Nova* **2000**, *23*, 346−356.

(26) Giusti, L.; Landaeta, V. R.; Vanni, M.; Kelly, J. A.; Wolf, R.; Caporali, M. Coordination Chemistry of Elemental Phosphorus. *Coord. Chem. Rev.* **2021**, *441*, 213927.

(27) Kelly, J. A.; Streitferdt, V.; Dimitrova, M.; Westermair, F. F.; Gschwind, R. M.; Berger, R. J.; Wolf, R. Transition-Metal-Stabilized Heavy Tetraphospholide Anions. *J. Am. Chem. Soc.* **2022**, *144*, 20434−20441.

(28) Russo, T. V.; Martin, R. L.; Hay, P. J. Effective Core Potentials for DFT Calculations. *J. Phys. Chem.* **1995**, *99*, 17085−17087.

(29) Peterson, K. A. Correlation Consistent Basis Sets for Actinides. I. The Th and U Atoms. *J. Chem. Phys.* **2015**, *142*, 074105.

(30) Cremer, D.; Zou, W.; Filatov, M. Dirac-exact relativistic methods: the normalized elimination of the small component method. *Wiley Interdiscip. Rev. Comput. Mol. Sci.* **2014**, *4*, 436−467.

(31) Zou, W.; Filatov, M.; Cremer, D. Analytical Energy Gradient for the Two-Component Normalized Elimination of the Small Component Method. *J. Chem. Phys.* **2015**, *142*, 214106.

(32) Zou, W.; Guo, G.; Suo, B.; Liu, W. Analytic Energy Gradients and Hessians of Exact Two-Component Relativistic Methods: Efficient Implementation and Extensive Applications. *J. Chem. Theory Comput.* **2020**, *16*, 1541−1554.

(33) Makoś, M. Z.; Zou, W.; Freindorf, M.; Kraka, E. Metal-Ring Interactions in Actinide Sandwich Compounds: A Combined Normalized Elimination of the Small Component and Local Vibrational Mode Study. *Mol. Phys.* **2020**, *118*, No. e1768314.

(34) Yoshizawa, T.; Zou, W.; Cremer, D. Calculations of Atomic Magnetic Nuclear Shielding Constants Based on the Two-Component Normalized Elimination of the Small Component Method. *J. Chem. Phys.* **2017**, *146*, 134109.

(35) Yoshizawa, T.; Filatov, M.; Cremer, D.; Zou, W. Calculation of Contact Densities and Mössbauer Isomer Shifts Utilising the Dirac-exact Two-component Normalised Elimination of the Small Component (2c-NESC) Method. *Mol. Phys.* **2019**, *117*, 1164−1171.

(36) Zou, W.; Filatov, M.; Cremer, D. Analytic Calculation of Second-Order Electric Response Properties with the Normalized Elimination of the Small Component (NESC) Method. *J. Chem. Phys.* **2012**, *137*, 084108.

(37) Zou, W.; Filatov, M.; Cremer, D. Development, Implementation, and Application of an Analytic Second Derivative Formalism for the Normalized Elimination of the Small Component Method. *J. Chem. Theory Comput.* **2012**, *8*, 2617−2629.

(38) Filatov, M.; Zou, W.; Cremer, D. Spin-orbit coupling calculations with the two-component Normalized Elimination of the Small Component Method. *J. Chem. Phys.* **2013**, *139*, 014106.

https://doi.org/10.1021/acs.inorgchem.3c01761
Inorg. Chem. 2023, 62, 12510−12524

(39) Filatov, M.; Zou, W.; Cremer, D. Calculation of Response Properties with the Normalized Elimination of the Small Component Method. *Int. J. Quantum Chem.* **2013**, *114*, 993−1005.
(40) Cheng, L.; Gauss, J. Analytic energy gradients for the spin-free exact two-component theory using an exact block diagonalization for the one-electron Dirac Hamiltonian. *J. Chem. Phys.* **2011**, *135*, 135.
(41) Cheng, L.; Gauss, J. Analytic Second Derivatives for the Spin-free Exact Two-component Theory. *J. Chem. Phys.* **2011**, *135*, 244104.
(42) Dyall, K. G. An Exact Separation of the Spin-free and Spin-dependent Terms of the Dirac−Coulomb−Breit Hamiltonian. *J. Chem. Phys.* **1994**, *100*, 2118−2127.
(43) Peng, D.; Liu, W.; Xiao, Y.; Cheng, L. Making Four-and Two-Component Relativistic Density Functional Methods Fully Equivalent Based on the Idea of "From Atoms to Molecule". *J. Chem. Phys.* **2007**, *127*, 104106.
(44) Costa Peluzo, B. M. T.; Kraka, E. Uranium: The Nuclear Fuel Cycle and Beyond. *Int. J. Mol. Sci.* **2022**, *23*, 4655.
(45) Konkoli, Z.; Cremer, D. A New Way of Analyzing Vibrational Spectra. I. Derivation of Adiabatic Internal Modes. *Int. J. Quantum Chem.* **1998**, *67*, 1−9.
(46) Wilson, E. B.; Decius, J. C.; Cross, P. C. *Molecular Vibrations: The Theory of Infrared and Raman Vibrational Spectra*; Courier Corporation, 1980.
(47) Wilson, E. B. Some Mathematical Methods for the Study of Molecular Vibrations. *J. Chem. Phys.* **1941**, *9*, 76−84.
(48) Zou, W.; Cremer, D. C_2 in a Box: Determining its Intrinsic Bond Strength for the X1Σg+Ground State. *Chem.—Eur. J.* **2016**, *22*, 4087−4099.
(49) Verma, N.; Tao, Y.; Zou, W.; Chen, X.; Chen, X.; Freindorf, M.; Kraka, E. A Critical Evaluation of Vibrational Stark Effect (VSE) Probes with the Local Vibrational Mode Theory. *Sensors* **2020**, *20*, 2358.
(50) Kraka, E.; Quintano, M.; La Force, H. W.; Antonio, J. J.; Freindorf, M. The Local Vibrational Mode Theory and Its Place in the Vibrational Spectroscopy Arena. *J. Phys. Chem. A* **2022**, *126*, 8781−8798.
(51) Kraka, E.; Zou, W.; Tao, Y. Decoding Chemical Information from Vibrational Spectroscopy Data: Local Vibrational Mode Theory. *Wiley Interdiscip. Rev. Comput. Mol. Sci.* **2020**, *10*, 1480.
(52) Zou, W.; Freindorf, M.; Oliveira, V.; Tao, Y.; Kraka, E. Weak and Strong π Interactions Between Two Monomers − Assessed With Local Vibrational Mode Theory. *Can. J. Chem.* **2022**, *00*, 1−18.
(53) Cremer, D.; Kraka, E. From Molecular Vibrations to Bonding, Chemical Reactions, and Reaction Mechanism. *Curr. Org. Chem.* **2010**, *14*, 1524−1560.
(54) Kraka, E.; Larsson, J. A.; Cremer, D. Generalization of the Badger Rule Based on the Use of Adiabatic Vibrational Modes. In *Computational Spectroscopy*; Grunenberg, J., Ed.; Wiley: New York, 2010; pp 105−149.
(55) Mayer, I. Charge, bond order and valence in the AB initio SCF theory. *Chem. Phys. Lett.* **1983**, *97*, 270−274.
(56) Mayer, I. Bond Orders and Valences From ab initio Wave Functions. *Int. J. Quantum Chem.* **1986**, *29*, 477−483.
(57) Mayer, I. Bond Order and Valence Indices: A Personal Account. *J. Comput. Chem.* **2007**, *28*, 204−221.
(58) Lyon, J. T.; Andrews, L.; Malmqvist, P.-Å.; Roos, B. O.; Yang, T.; Bursten, B. E. Infrared Spectrum and Bonding in Uranium Methylidene Dihydride, CH_2UH_2. *Inorg. Chem.* **2007**, *46*, 4917−4925.
(59) Roos, B. O.; Lindh, R.; Cho, H.-G.; Andrews, L. Agostic Interaction in the Methylidene Metal Dihydride Complexes H_2MCH_2 (M= Y, Zr, Nb, Mo, Ru, Th, or U). *J. Phys. Chem. A* **2007**, *111*, 6420−6424.
(60) Bader, R. F. W. Atoms in Molecules. *Acc. Chem. Res.* **1985**, *18*, 9−15.
(61) Bader, R. *Atoms in Molecules: A Quantum Theory; International Series of Monographs on Chemistry*; Clarendon Press: Oxford, 1990.
(62) Bader, R. *Atoms in Molecules: A Quantum Theory*; Clarendron Press: Oxford, 1995.
(63) Popelier, P. *Atoms in Molecules: An Introduction*; Prentice-Hall: Harlow, England, 2000.
(64) Cremer, D.; Kraka, E. Chemical Bonds without Bonding Electron Density? Does the Difference Electron-Density Analysis Suffice for a Description of the Chemical Bond? *Angew. Chem., Int. Ed.* **1984**, *23*, 627−628.
(65) Cremer, D.; Kraka, E. A Description of the Chemical Bond in Terms of Local Properties of Electron Density and Energy. *Croat. Chem. Acta* **1984**, *57*, 1259−1281.
(66) Kraka, E.; Cremer, D. Chemical Implication of Local Features of the Electron Density Distribution In *Theoretical Models of Chemical Bonding: The Concept of the Chemical Bond*; Maksic, Z. B., Ed.; Springer Verlag: Heidelberg, 1990; Vol. 2, pp 453−542.
(67) Tassell, M. J.; Kaltsoyannis, N. Covalency in $AnCp_4$ (An=Th-Cm): A Comparison of Molecular Orbital, Natural Population and Atoms-in-molecules Analyses. *Dalton Trans.* **2010**, *39*, 6719.
(68) Perdew, J. P.; Burke, K.; Ernzerhof, M. Generalized Gradient Approximation Made Simple. *Phys. Rev. Lett.* **1996**, *77*, 3865−3868.
(69) Adamo, C.; Barone, V. Toward Reliable Density Functional Methods Without Adjustable Parameters: The PBE0 Model. *J. Chem. Phys.* **1999**, *110*, 6158−6170.
(70) Ernzerhof, M.; Scuseria, G. E. Assessment of the Perdew−Burke−Ernzerhof exchange-correlation functional. *J. Chem. Phys.* **1999**, *110*, 5029−5036.
(71) Pantazis, D. A.; Neese, F. All-electron Scalar Relativistic Basis Sets for the Actinides. *J. Chem. Theory Comput.* **2011**, *7*, 677−684.
(72) Dunning, T. H. Gaussian basis sets for use in correlated molecular calculations. I. The atoms boron through neon and hydrogen. *J. Chem. Phys.* **1989**, *90*, 1007−1023.
(73) Woon, D. E.; Dunning, T. H. Gaussian Basis Sets For Use in Correlated Molecular Calculations. III. The Atoms Aluminum Through Argon. *J. Chem. Phys.* **1993**, *98*, 1358−1371.
(74) Pritchard, B. P.; Altarawy, D.; Didier, B.; Gibson, T. D.; Windus, T. L. New Basis Set Exchange: An Open, Up-to-Date Resource for the Molecular Sciences Community. *J. Chem. Inf. Model.* **2019**, *59*, 4814−4820.
(75) Feller, D. The role of databases in support of computational chemistry calculations. *J. Comput. Chem.* **1996**, *17*, 1571−1586.
(76) Schuchardt, K. L.; Didier, B. T.; Elsethagen, T.; Sun, L.; Gurumoorthi, V.; Chase, J.; Li, J.; Windus, T. L. Basis Set Exchange: A Community Database for Computational Sciences. *J. Chem. Inf. Model.* **2007**, *47*, 1045−1052.
(77) Kraka, E.; Cremer, D.; Zou, W.; Filatov, M.; Gräfenstein, J.; Izotov, D.; Gauss, J.; He, Y.; Wu, A.; Konkoli, Z.; Polo, V.; Olsson, L.; He, Z. COLOGNE2020 Computational and Theoretical Chemistry Group (CATCO). Ph.D. Thesis, Southern Methodist University, Dallas, TX, USA, 2020.
(78) Fisch, M.; et al. *Gaussian 16*, Revision B. 01; Gaussian. Inc.: Wallingford, CT, 2016.
(79) Weinhold, F.; Landis, C.; Valency, B. *A Natural Bond Orbital Donor-Acceptor Perspective*; University of Wisconsin: Madison, 2005; p 317.
(80) Martins, L. S. C.; Jorge, F. E.; Franco, M. L.; Ferreira, I. B. All-electron Gaussian Basis Sets of Double Zeta Quality For the Actinides. *J. Chem. Phys.* **2016**, *145*, 244113.
(81) Weinhold, F.; Landis, C. R. *Valency and Bonding: A Natural Bond Orbital Donor-Acceptor Perspective*; Cambridge University Press, 2005.
(82) Zou, W.; Tao, Y.; Freindorf, M.; Makoś, M. Z.; Verma, N.; Cremer, D.; Kraka, E. Local Vibrational Mode Analysis (LModeA. Computational and Theoretical Chemistry Group (CATCO). Ph.D. Thesis, Southern Methodist University, Dallas, TX, USA, 2022.
(83) Keith, T. A. *AIMALL. TK Gristmill Software*: Overland Park KS, 2017.
(84) Kraka, E.; Cremer, D. Weaker Bonds with Shorter Bond Lengths. *Rev. Proc. Quim.* **2012**, *6*, 31−34.
(85) Sexton, T.; Kraka, E.; Cremer, D. Extraordinary Mechanism of the Diels-Alder Reaction: Investigation of Stereochemistry, Charge

https://doi.org/10.1021/acs.inorgchem.3c01761
Inorg. Chem. 2023, 62, 12510−12524

Transfer, Charge Polarization, and Biradicaloid Formation. *J. Phys. Chem. A* **2016**, *120*, 1097−1111.
(86) Dutkiewicz, M. S.; Farnaby, J. H.; Apostolidis, C.; Colineau, E.; Walter, O.; Magnani, N.; Gardiner, M. G.; Love, J. B.; Kaltsoyannis, N.; Caciuffo, R.; et al. Organometallic neptunium(III) complexes. *Nat. Chem.* **2016**, *8*, 797−802.
(87) Kirker, I.; Kaltsoyannis, N. Does Covalency Really Increase Across the 5f Series? A Comparison of Molecular Orbital, Natural Population, Spin and Electron Density Analyses of $AnCp_3$ (An=Th−Cm; Cp=η^5-C_5H_5). *Dalton Trans.* **2011**, *40*, 124−131.
(88) Kraka, E.; Cremer, D. Description of Chemical Reactions in Terms of the Properties of the Electron Density. *J. Mol. Struct.: THEOCHEM* **1992**, *255*, 189−206.
(89) Maynadié, J.; Barros, N.; Berthet, J. C.; Thuéry, P.; Maron, L.; Ephritikhine, M. The Crucial Role of the f Electrons in the Bent or Linear Configuration of Uranium Cyanido Metallocenes. *Angew. Chem., Int. Ed.* **2007**, *46*, 2010−2012.
(90) Bent, H. A. Distribution of Atomic s Character in Molecules and its Chemical Implications. *J. Chem. Educ.* **1960**, *37*, 616.

https://doi.org/10.1021/acs.inorgchem.3c01761
Inorg. Chem. 2023, 62, 12510−12524